



Millimeter-VLBI Observations of Low-luminosity Active Galactic Nuclei with Source-frequency Phase Referencing

Wu Jiang^{1,2}, Zhiqiang Shen^{1,2}, Ivan Martí-Vidal³, Xuezheng Wang^{1,4}, Dongrong Jiang^{1,2}, and Noriyuki Kawaguchi⁵

¹Shanghai Astronomical Observatory, Chinese Academy of Sciences, Shanghai 200030, People's Republic of China; jiangwu@shao.ac.cn

²Key Laboratory of Radio Astronomy, Chinese Academy of Sciences, Nanjing 210008, People's Republic of China

³Department of Astronomy and Astrophysics, University of Valencia, E-46100, Burjassot, Spain

⁴ShanghaiTech University, 393 Middle Huaxia Road, Pudong, Shanghai, 201210, People's Republic of China

⁵National Astronomical Observatory of Japan, 2-21-1 Osawa, Mitaka, Tokyo 181-8588, Japan

Received 2021 September 10; revised 2021 November 7; accepted 2021 November 8; published 2021 November 19

Abstract

We report millimeter-VLBI results of low-luminosity active galactic nuclei (M84 and M87) up to 88 GHz with source-frequency phase-referencing observations. We detected the weak VLBI core and obtained the first image of M84 at 88 GHz. The derived brightness temperature of the M84 core was about 7.2×10^9 K, which could serve as a lower limit because the core down to 30 Schwarzschild radii was still unresolved in our 88 GHz observations. We successfully determined the core shifts of M87 at 22–44 GHz and 44–88 GHz through the source-frequency phase-referencing technique. The jet apex of M87 could be deduced at $\sim 46 \mu\text{as}$ upstream of the 43 GHz core from core-shift measurements. The estimated magnetic field strength of the 88 GHz core of M87 is 4.8 ± 2.4 G, which is at the same magnitude of 1–30 G near the event horizon probed by the Event Horizon Telescope.

Unified Astronomy Thesaurus concepts: [Low-luminosity active galactic nuclei \(2033\)](#); [Very long baseline interferometry \(1769\)](#)

1. Introduction

The low-luminosity active galactic nuclei (LLAGNs) classified by their low bolometric luminosities and sub-Eddington accretion rates commonly exist in nearby galaxies (Nagar et al. 2002; Ho 2008). Unlike their bright cousins, the broadband spectral energy distributions prefer the model of an inner advection-dominated accretion flow and an outer truncated thin disk (Yu et al. 2011; Nemmen et al. 2014). Meanwhile, compact flat-spectrum radio cores were detected in LLAGNs (Nagar et al. 2002) and suggested to be scaled-down versions of AGN jets (Falcke & Biermann 1999). The fact that it hosts a large mass central supermassive black hole, and its proximity, make LLAGN approachable to the launching and acceleration regions of the inner jet, even to its event horizon at millimeter or submillimeter wavelengths.

According to the inhomogeneous model of the relativistic jet, the position of the VLBI core is frequency dependent. This frequency-dependent shift in the location of the core (core-shift) can be used to estimate the magnetic field strength and electron number density of the jet (Lobanov 1998; Kovalev et al. 2008). However, only a few active galactic nuclei (AGNs) have reliable core-shift measurements at millimeter wavelengths (O’Sullivan & Gabuzda 2009). The core-shift measurements are mostly obtained at low frequencies due to limited sensitivity at high frequencies (Pushkarev et al. 2012). Although millimeter-VLBI can approach the inner region of the jet as the plasma turns optically thin at high frequency, the core shift is difficult to obtain due to the rapid phase fluctuations of the atmosphere and thus limited coherent integration time for the conventional VLBI phase-referencing observations. Fortunately, a newly proposed VLBI phase-referencing technique called source-frequency

phase referencing (SFPR) can be used to measure the core-shift effect (Rioja & Dodson 2011), essentially being of great advantage at millimeter wavelengths. We successfully obtained the first VLBI image of the LLAGN M81* at 88 GHz and measured the shift between 7 and 3 mm wavelengths in the compact jet (Jiang et al. 2018).

In this paper, we will present the applications of SFPR to two LLAGNs, M84 and M87. The observation summary and data reduction are presented in Section 2. The results are in Section 3, followed by the conclusion in Section 4.

2. Observations and Data Reduction

2.1. Observations

The observations of M84 and M87 were carried out with the VLBA in SFPR mode on 2019 June 22, with a 22 and 44 GHz frequency pair. The observations with a 44 and 88 GHz frequency pair were first performed on 2019 June 18, but most stations failed at 88 GHz. Therefore it was reobserved on 2021 March 31, for satisfied weather conditions at most stations. The on-source time of each source per scan was ~ 30 seconds at a frequency. A fast frequency-switching cycle of two frequencies on a source was taken as a loop. M87 ($\sim 1.5^\circ$ apart from M84 in the sky) was interleaved every five loops of M84 for the 22/44 GHz epoch and nine loops for the 44/88 GHz epoch. Several loops of blazar 1219+044 were observed at the beginning and the end of observations but not included here, due to rapid phase fluctuations of low antenna elevation angles. The 2019 epoch was recorded at 2048 Mbps by splitting the 512 MHz total bandwidth into 16 intermediate frequency (IF) bands while the 2021 epoch was at 4096 Mbps by splitting 1024 MHz bandwidth into eight IFs.

2.2. Data Reduction

The data calibration and reduction followed the procedures in Rioja & Dodson (2011) and Jiang et al. (2018). First we performed standard amplitude and phase calibrations in AIPS for

Table 1
Summary of VLBI Image Parameters of M84 and M87 in the Observations

No.	Epoch	Frequency GHz	Synthesized Beam on M84/M87			
			Major Axis mas	Minor Axis mas	Position Angle degree	R.A. Component mas
(1)	(2)	(3)	(4)	(5)	(6)	(7)
1	2019-06-22	21.9	1.49/1.26	0.41/0.37	$-14^{\circ}5' / -20^{\circ}5'$	0.42/0.39
2	2019-06-22	43.8	0.63/0.57	0.22/0.21	$-15^{\circ}6' / -20^{\circ}4'$	0.23/0.22
3	2021-03-31	43.8	0.60/0.53	0.24/0.22	$-18^{\circ}0' / -22^{\circ}7'$	0.25/0.24
4	2021-03-31	87.5	0.29/0.27	0.16/0.15	$-11^{\circ}0' / -19^{\circ}6'$	0.16/0.16

Note. Column (1): number of VLBI images at different epochs and observing frequencies. Columns (2)–(3): observing date and frequency. Columns (4)–(6): the parameters (major axis, minor axis, and position angle) of the nominal synthesized beam at each frequency. Column (7): the beam size in the R.A. direction (R.A. component) of the nominal synthesized beam at each frequency.

both M84 and M87 at the reference frequencies (22 GHz of 2019 epoch and 44 GHz of 2021 epoch), respectively. Their images were obtained by further clean and self-calibration in Difmap. Second the corresponding phase solutions of the AIPS task FRING after taking into account clean models of M84 and M87 were multiplied by a factor of 2, while the delay and delay rate solutions were unchanged. These revised solutions were then applied to the target frequencies (44 GHz in 2019 epoch and 88 GHz in 2021 epoch, respectively), which is called the frequency phase transfer (FPT) calibration. The phase fluctuations in proportion to the observing frequency such as the unmodeled tropospheric and geometric errors were eliminated in this step. Third the SFPR-ed images of M84 at target frequencies were obtained by further phase referencing to the FRING solutions of the FPT calibrated data of M87 at the same target frequencies, which refined the unmodeled dispersive ionospheric and instrumental errors. The corresponding core-shift measurements were derived from the SFPR-ed images using JMFIT in AIPS. Finally high-resolution VLBI images of M84 were obtained by clean and self-calibration in Difmap (Jiang et al. 2018).

Since the brightness-peak position of the image is usually referred to as the core position, the prominent jet of M87 in the R.A. direction would cause the peak position to be slightly offset from the “true core” position toward the downstream side, due to the blending of near-core jet emission within the finite beam size. To evaluate this effect, we used the method in Hada et al. (2014), convolving the M87 structure by different beam size with diameters ranging from the minor axis of the nominal synthesized beam (shown in Table 1), whose direction was almost in the R.A. direction in our observations, to about 4 times larger. Then, we plotted systematic changes of the brightness-peak position as a function of beam size. In the case of 22 GHz, the image was restored with beam sizes ranging from 0.3 to 1.2 milliarcsecond (mas) in incremental steps of 0.1 mas. We found a progressive position shift of the brightness peak toward the downstream to be 10 microarcsecond (μas) per 0.1 mas in the R.A. direction. In the case of 44 GHz, the image was restored with beam sizes ranging from 0.2 to 0.8 mas in incremental steps of 0.1 mas. The position shift of the brightness peak toward the downstream was $6.8 \mu\text{as}$ per 0.1 mas in the R.A. direction. In the case of 88 GHz, the image was restored with beam sizes ranging from 0.15 to 0.6 mas in incremental steps of 0.05 mas. The position shift of the brightness peak toward the downstream was $2.5 \mu\text{as}$ per 0.1 mas in the R.A. direction. That means the “true core” position would be shifted to upstream, with respect to the brightness-peak position when convolved with a nominal

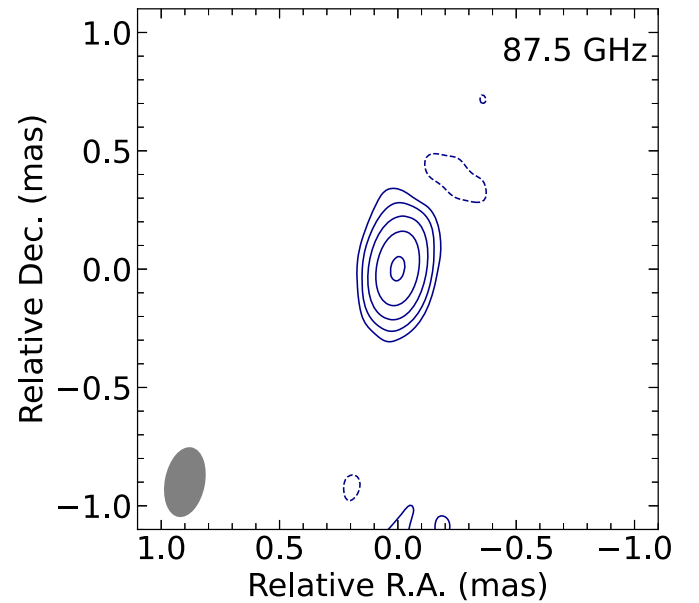


Figure 1. Natural-weighted SFPR-ed VLBI image of M84 at 88 GHz after self-calibration. The peak flux density is $38.1 \text{ mJy beam}^{-1}$. The contour levels are at $2.2 \times (-1, 1, 2, 4, 8, 16) \text{ mJy beam}^{-1}$. The lowest level is 3 times the rms noise of the image. The beam indicated in the left bottom corner is $0.29 \text{ mas} \times 0.16 \text{ mas}$ at -11° .

beam. At 22 GHz, the upstream shift in the R.A. direction would be about $10 \times 0.39 \text{ mas} / 0.1 \text{ mas} = 39 \mu\text{as}$. At 44 GHz, it would be about $6.8 \times 0.22 \text{ mas} / 0.1 \text{ mas} = 15 \mu\text{as}$ for the 2019 epoch, and about $6.8 \times 0.24 \text{ mas} / 0.1 \text{ mas} = 16 \mu\text{as}$ for the 2021 epoch. At 88 GHz, it was about $2.5 \times 0.16 \text{ mas} / 0.1 \text{ mas} = 4 \mu\text{as}$. Where 0.39 mas , 0.22 mas , 0.24 mas , and 0.16 mas were the nominal beam sizes in the R.A. direction (see Table 1). Consequently, the measured core shift in the R.A. direction from the peak-positions would be about $39 - 15 = 24 \mu\text{as}$ larger than the “true core shift” in magnitude at 22–44 GHz and, $16 - 4 = 12 \mu\text{as}$ larger at 44–88 GHz.

2.3. Error Analysis

The error budgets of SFPR mainly include the dynamic tropospheric error, the core identification error of M87 and the statistical error from images. These errors are independent of each other and the total errors can be calculated as their root-sum-square. We adopt $11 \mu\text{as}$ for the dynamic tropospheric error among frequencies under relatively stable weather conditions, assuming 0.01 m uncanceled error by the water vapor fluctuation

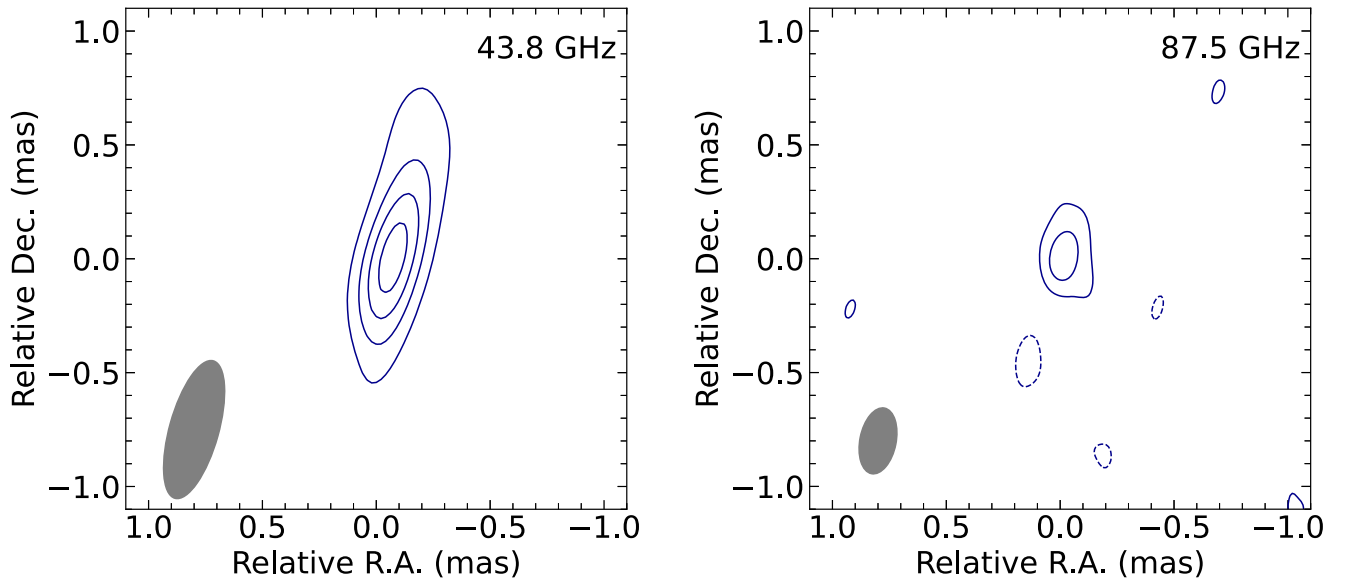


Figure 2. SFPR-ed images of M84 at 44 (left) and 88 GHz (right) on 2019 June 22 and 2021 March 31, respectively. The peak intensity is 4.1 and 8.2 mJy beam⁻¹, respectively. The contour levels are at -3, 3, 6, 9, and 12 times the rms of the images (0.3 and 1.0 mJy beam⁻¹). The FWHM of the convolving beams (0.63 mas × 0.22 mas at -15°6 and 0.29 mas × 0.16 mas at -11°3) are shown in gray in the bottom left corners of each image.

as that in Hada et al. (2011). The absolute tropospheric position error for a single frequency can be significantly larger than this value, while most of the error can be canceled out by the FPT calibration in SFPR observations. We also performed the error analysis for the core identification error of M87 as in Hada et al. (2011), using the core position differences between two methods. One defined the centroid of the elliptical Gaussian fitting M87 core region as the core position, the other is the brightness-peak position of the images convolved with a circular Gaussian beam of about a half of a synthesized beam in the core-jet direction. The uncertainties of core identification of M87 in the R.A. direction are 7 μ as and 6 μ as at 22 GHz and 44 GHz for the 2019 epoch, respectively. They were 5 μ as and 3 μ as at 44 GHz and 88 GHz for the 2021 epoch, respectively. Since the SFPR-ed images coupled the errors from both frequencies, the statistical error at each frequency was $1/\sqrt{2}$ of the beam size divided by the signal-to-noise ratios of the SFPR-ed image. It was 12 μ as at 22 and 44 GHz for the 2019 epoch, 14 μ as at 44 GHz, and 88 GHz for the 2021 epoch. The intrinsic structural uncertainty of M84 would also affect the core shift of M87. In our observations, the position angles of fitting to the core region of M84 at 22 and 44 GHz with an elliptical Gaussian were within 5 degrees in the north. Therefore the uncertainties of the core-shift effect in M84 in the R.A. direction were 5 μ as, 3 μ as, and 2 μ as at 22, 44, and 88 GHz, respectively. Other minor errors such as the ionospheric residuals and geometric errors at each frequency were taken as the empirical values (Hada et al. 2011). The total errors by the root-sum-square of all the above uncertainties give 19 μ as and 18 μ as at 22 and 44 GHz for the 2019 epoch and 19 μ as and 18 μ as at 44 and 88 GHz for the 2021 epoch, respectively.

3. Results and Discussion

3.1. VLBI Core of M84 at 3 mm

The nearby elliptical galaxy M84 is located in the center of the Virgo Cluster at a distance of 18.5 Mpc ($z = 0.00339$) and has a central supermassive black hole weighing $\sim 8.5 \times 10^8 M_{\odot}$. The combination of its proximity and a large black hole mass

yields a privileged linear resolution conversion factor down to 1 μ as ~ 1 Schwarzschild radii (R_S), allowing us to investigate its close vicinity of the supermassive black hole with VLBI. Two side jets are seen at a large viewing angle of $\sim 74^\circ$ (Meyer et al. 2018). The image of M84 at 88 GHz (Figure 1) was obtained by performing further clean and self-calibration in phase only to the SFPR-ed visibility data, which were scan averaged. The MODELFIT task in Difmap was used to fit the calibrated visibility with circular Gaussian components. The VLBI core of M84 could be fitted by a circular Gaussian with a flux density of 38.0 ± 5.7 mJy and a diameter of 29 ± 11 μ as well. The apparent brightness temperature of the core (Kim et al. 2018), $T_{b,app}$, can be calculated by

$$T_{b,app} = 1.22 \times 10^{12} \frac{S_{core}(1+z)}{\nu^2 \theta_{core}^2} K, \quad (1)$$

where S_{core} is the core flux density in Jy, ν is the observing frequency in GHz, θ_{core} is the equivalent size in mas, and z is the redshift. The $T_{b,app}$ of the M84 core at 88 GHz is $\sim 7.2 \times 10^9$ K. Similar to other LLAGNs (Kim et al. 2018), and the $T_{b,app}$ is generally quite low. The derived brightness temperature could serve as a lower limit as the core size of 29 μ as (30 R_S) was only one-tenth of the beam size and still unresolved in our 88 GHz observations.

3.2. Core Shift of M87

M87 is the most prominent elliptical galaxy within the Virgo Cluster, located at a distance of 16.8 ± 0.8 Mpc away. Its central supermassive black hole ($\sim 6.5 \times 10^9 M_{\odot}$) and jet have been well-studied in almost every wave band from radio to γ -rays (Event Horizon Telescope Collaboration et al. 2019; EHT MWL Science Working Group et al. 2021). The core shift of M87 up to 43 GHz has been measured through conventional phase referencing to M84 (Hada et al. 2011, 2013). The core shift in the R.A. direction $r_{R.A.}(\nu)$ followed $\nu^{-0.94}$ and indicated that the black hole was located at ~ 41 μ as eastwards of the 43 GHz core (Hada et al. 2011). The core shifts at 22–44 GHz and 44–88 GHz could

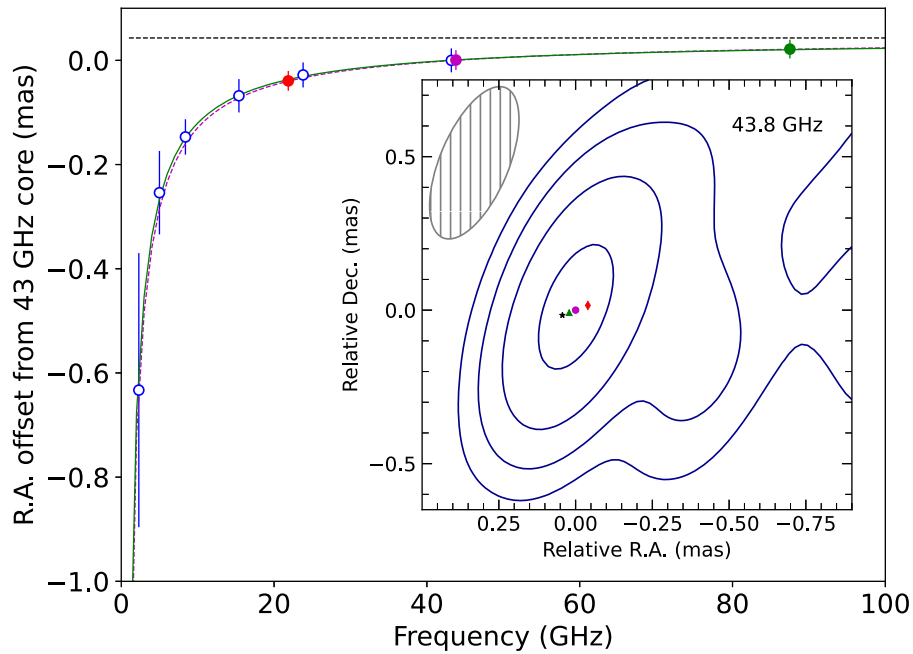


Figure 3. Offsets in R.A. with respect to observing frequency from 43 GHz core in M87. The data in hollow circles are from Hada et al. (2011). The solid circles are the measurements in this work. The fitting of these two data sets with the same formula as Hada et al. (2011) is shown by the green curve, indicating the jet apex position of $43 \mu\text{as}$ in R.A. (black dashed line). The fitting to the data of this work only is the dashed curve in magenta. The subplot in the bottom right corner shows the core positions at 22, 44, and 88 GHz and the jet apex, which are marked as diamond, circle, triangle, and star, respectively, overlapping with the VLBI image of M87 at 44 GHz in 2021. The contour levels are at $12.0 \text{ mJy beam}^{-1}$ (27σ noise level of the image) stepping by a factor of 3, the beam in gray is $0.53 \text{ mas} \times 0.22 \text{ mas}$ at $-22^\circ 7'$.

Table 2
Fitting the Location of Jet Apex in M87

No.	Core-shift Data Used	$r_{\text{R.A.}} = A\nu^{-k} + B$		
		A	k	B
(1)	(2)	(3)	(4)	(5)
1	This work	-1.45	0.92	0.045
2	Hada et al. (2011) and this work	-1.36 ± 0.15	0.92 ± 0.06	0.043 ± 0.007

Note. Column (1): number of the fitting. Column (2): core-shift measurements used. Columns (3)–(5): fitting parameters A , k , and B . B is the offset of the jet apex in the R.A. direction from the 43 GHz core.

be obtained from the SFPR-ed images (Rioja & Dodson 2011; Jiang et al. 2018) as shown in Figure 2. Since the jet extended structure of M84 is toward the north direction, the core shift of M84 in the R.A. direction could be negligible. The core shift of M87 in the R.A. direction could be obtained from the SFPR-ed images by Equation (2) in Jiang et al. (2018). As a result, we obtained a position shift in the R.A. direction of $-64 \pm 8 \mu\text{as}$ at the 22 GHz core with regard to the 44 GHz core, and of $-33 \pm 11 \mu\text{as}$ at 44–88 GHz. The error in 1σ was given by JMFIT in AIPS. After taking into account of the blending effect of near-core jet emission in M87 (see Section 2.2), the “true core shift” would be about $-(64-24) = -40 \mu\text{as}$ at 22–44 GHz and $-(33-12) = -21 \mu\text{as}$ at 44–88 GHz. Incorporating the uncertainties given by error analysis (see Section 2.3), the core positions relative to that of the 44 GHz core in R.A. was $-40 \pm 19 \mu\text{as}$ at 22 GHz for the 2019 epoch and $21 \pm 18 \mu\text{as}$ at 88 GHz for the 2021 epoch, respectively.

Using the same formula $r_{\text{R.A.}}(\nu) = A\nu^{-k} + B$ in Hada et al. (2011), the abovementioned two core shifts in the R.A. direction could be solved with solutions $A = -1.45$, $k = 0.92$, and $B = 0.045$. As presented in the bottom right corner of Figure 3, assuming a jet position angle of -69° with respect to north in M87 (Kim et al. 2018), B value indicates that the jet apex is located at $\sim 48 \mu\text{as}$ upstream of the 43 GHz core. It was consistent with the previous result of $44 \pm 13 \mu\text{as}$ in Hada et al. (2011). Since there was no strong flare event to cause the core-shift variations (Plavin et al. 2019) during our observations as well as in the Hada et al. (2011) session, it would be reasonable to align the 43 GHz core positions of M87 among these sessions. The core shift in R.A. at 22–43 GHz even during the elevated very high energy gamma-ray state in 2012 was found to be also at a similar level ($\sim 10 \mu\text{as}$ larger; Hada et al. 2014). Furthermore, aligning the 43 GHz cores among Hada et al. (2011) and the two epochs of this work, we fitted these combined core-shift measurements with the weighted least-squares method. It gave out $A = -1.36 \pm 0.15$, $k = 0.92 \pm 0.06$, and $B = 0.043 \pm 0.007$ as shown in Table 2. The results are consistent and imply the jet apex is $43 \pm 7 \mu\text{as}$ in R.A. (as indicated by the black dashed line in Figure 3) or at $\sim 46 \mu\text{as}$ upstream of the 43 GHz core.

Following Equation (4) in Lobanov (1998), we could estimate the core-shift measure $\Omega_{r,22-44} = 0.13 \pm 0.06$ [pc GHz] and $\Omega_{r,44-88} = 0.12 \pm 0.10$ [pc GHz], using the resultant power-law index $k_r = 1.09$. The magnetic field strength at the 88 GHz core is estimated to be 4.8 ± 2.4 G using the mean value of Ω_r , by Equation (B.2) in Paraschos et al. (2021) with a spectral index of -0.5 , a Doppler factor of 2, a jet viewing angle of 18° , and an intrinsic jet opening angle of $63^\circ 6'$ at 88 GHz (Kim et al. 2018). This is consistent with the estimated 1–30 G near the event horizon by the Event Horizon Telescope at 230 GHz (Event Horizon Telescope Collaboration et al. 2021).




4. Conclusions

We have successfully demonstrated that the SFPR technique could be applied to the mm-VLBI observations of LLAGNs. It helps to overcome the limited coherent integration time and has great advantages in detecting the weak VLBI core as well as measuring the core shift at millimeter wavelengths. The VLBI core of M84 at 88 GHz was detected and the lower limit of its apparent brightness temperature $\sim 7.2 \times 10^9$ K was obtained. By means of SFPR to M84, the core shift of M87 in the R.A. direction was determined at a precision of $\sim 20 \mu\text{as}$, which further constrained the jet apex at $\sim 46 \mu\text{as}$ upstream of the 43 GHz core. With the aid of simultaneous multifrequency receiving system and more stations available (Zhao et al. 2019; Rioja & Dodson 2020), SFPR will be a very powerful tool to investigate the compactness of the jet base at high frequencies as well as physical parameters such as core structure, brightness temperature, and magnetic field of the inner region of jet.

The authors thank the anonymous referee for very critical and constructive suggestions. This work was supported in part by the National Natural Science Foundation of China (grant Nos. 11803071, 11590780, 11590784, and 11933007) and Key Research Program of Frontier Sciences, CAS (grant No. QYZDJ-SSW-SLH057). VLBA is operated by the National Radio Astronomy Observatory, which is a facility of the National Science Foundation operated under cooperative agreement by Associated Universities, Inc.

ORCID iDs

Wu Jiang  <https://orcid.org/0000-0001-7369-3539>

Zhiqiang Shen  <https://orcid.org/0000-0003-3540-8746>
 Ivan Martí-Vidal  <https://orcid.org/0000-0003-3708-9611>
 Noriyuki Kawaguchi  <https://orcid.org/0000-0002-7776-3159>

References

- Event Horizon Telescope Collaboration, Akiyama, K., Alberdi, A., et al. 2019, *ApJL*, **875**, L1
- EHT MWL Science Working Group, Algaba, J. C., Anzarski, J., et al. 2021, *ApJL*, **911**, L11
- Event Horizon Telescope Collaboration, Akiyama, K., Algaba, J. C., et al. 2021, *ApJL*, **910**, L13
- Falcke, H., & Biermann, P. L. 1999, *A&A*, **342**, 49
- Hada, K., Doi, A., Kino, M., et al. 2011, *Natur*, **477**, 185
- Hada, K., Kino, M., Doi, A., et al. 2013, *ApJ*, **775**, 70
- Hada, K., Giroletti, M., Kino, M., et al. 2014, *ApJ*, **788**, 165
- Ho, L. C. 2008, *ARA&A*, **46**, 475
- Jiang, W., Shen, Z.-Q., Jiang, D.-r., Martí-Vidal, I., & Kawaguchi, N. 2018, *ApJL*, **853**, L14
- Kim, J.-Y., Krichbaum, T. P., Lu, R.-S., et al. 2018, *A&A*, **616**, A188
- Kovalev, Y. Y., Lobanov, A. P., Pushkarev, A. B., et al. 2008, *A&A*, **483**, 759
- Lobanov, A. P. 1998, *A&A*, **330**, 79
- Nagar, N. M., Falcke, H., Wilson, A. S., et al. 2002, *A&A*, **392**, 53
- Meyer, E. T., Petropoulou, M., Georganopoulos, M., et al. 2018, *ApJ*, **860**, 9
- Nemmen, R. S., Storchi-Bergmann, T., & Eracleous, M. 2014, *MNRAS*, **438**, 2804
- O'Sullivan, S. P., & Gabuzda, D. C. 2009, *MNRAS*, **400**, 26
- Paraschos, G. F., Kim, J.-Y., Krichbaum, T. P., et al. 2021, *A&A*, **650**, L18
- Plavin, A. V., Kovalev, Y. Y., Pushkarev, A. B., et al. 2019, *MNRAS*, **485**, 1822
- Pushkarev, A. B., Hovatta, T., Kovalev, Y. Y., et al. 2012, *A&A*, **545**, 133
- Rioja, M., & Dodson, R. 2011, *AJ*, **141**, 114
- Rioja, M. J., & Dodson, R. 2020, *A&ARv*, **28**, 6
- Yu, Z., Yuan, F., & Ho, L. C. 2011, *ApJ*, **726**, 87
- Zhao, G.-Y., Jung, T., Sohn, B. W., et al. 2019, *JKAS*, **52**, 23